Cancer Immunotherapy: Planning Report

Supervisors: Professor Reiko Tanaka, Doctor Tara Hameed

Alexandre Yann Péré
CID: 01938104
December 26, 2023

Contents

1 Project Specification

1.1 Background

1.1.1 Cancer

Cancer is a large class of diseases that is the second leading cause of death in the United-State [1]. While the immune system has the potential to target and eliminate cancer cells, cancer often finds ways to evade these natural defenses. [2]. Traditional methods, such as chemotherapy or surgery, rely on using destructive external agents to kill the cancerous cells. However, introducing foreign agents in the body often results in heavy side effects [cite]. This prompted the development of immunotherapies, a type of treatment aimed at countering cancer's ability to escape immune detection, which thus has the potential to be less toxic. Several viable strategies exist for immunotherapy. The specific treatment of concern in this project is a triple combination of acytokine-based treatment and with two immune checkpoint inhibitors. We will first review the general principles behind these stratgeies.

1.1.2 Immunotherapies

Cytokine-based Therapies

Cytokine-based therapies rely on the injection of specific cytokines (small proteins that act as signalling molecules during the immune response) to control tumour growth [3]. One of the most promising cytokine thus far is the interleukin-12 (IL-12), that was shown to have potent antitumour effects [4]. While it does not directly affect tumour cells, it mediates the production of other molecules or cells that have a more direct effect [5]. First of all, it activates the production of tumour-infiltrating cytotoxic cells, mainly $CD8^+$ [6]. These are a type of T-lymphocytes whose main function is to carry out cytotoxic activity (i.e. killing the malignant cells) after detecting tumoural antigen [7]. Secondly, they induce production of another type of cytokine, called interferon-γ (IFNγ). IFNg in turn affects the tumour microenvironment by stimulating production of cytotoxic cells [8], reducing angiogenesis [9] and upregulating antigen-presenting pathways within tumour cells [10]. Lastly, IL-12 facilitates T-cell proliferation (including $CD8^+$) by reducing negative regulatory pathways that lead to immunosuppression [11]. It does so by inhibiting the effect of immune checkpoint Programmed Death 1 (PD1), following a similar strategy to checkpoint inhibitor (CPI) treatments (the more detailed mode of action is described in the following paragraph). While these three pathways indicate that IL-12 has a very robust antitumour effect, clinical studies demonstrated that systemic injection of IL-12 is exceedingly toxic as it triggers a large immune response throughout the whole body [cite]. These severe treatment-related adverse effects (TRAEs) dampened research about IL-12, waiting for a safer, more localised delivery method to be found.

Immune Checkpoint Inhibitors

The usual partner of cytokine-based treatments are checkpoint inhibitors. To understand checkpoint inhibition, we must first review in more detail the negative regulatory pathways of $CD8^+$ T-cells activity. The most potent pathway involves checkpoint molecules, either Cytotoxic T-lymphocyte antigen 4 (CTLA4) or programmed cell death 1 (PD1) [12]. Both molecules are membrane protein receptors that act with some delay to exhaust and deactivate T-cell functions after they are stimulated by antigen-presenting cells (APC). Both CTLA4 and PD1 function in similar ways, the main difference being the type of tissues they affect [13]. Although their original function was shown to be prevention of autoimmunity [14], they lead to immunosuppression in the presence of tumours. The idea of inhibiting these regulators to shift the tumour microenvironment away from immunosuppression hence seemed natural, and this is precisely the

idea behind CPI treatments. Clinical trials demonstrated positive results in several types of cancers [cite], but performed poorly against immunologically cold tumours, i.e. tumour that do not normally elicit a strong immune response (they escape the immune system very effectively), such as melanoma [cite].

1.2 Motivation

Recent endeavours in this field of immunotherapies led to the development by Mansurov, Ishihara et al. of a new molecule, CBD-IL-12, that demonstrated promising results to treat melanoma [15]. The CBD-IL-12 molecule consists of a collagen-binding protein (or collagen-binding domain, CBD) that is fused onto a IL-12 cytokine. The modified interleukin hence mainly accumulates in collagen-rich regions. As collegen is the main component of cancerous microenvironment [16], this effectively results in an enhanced delivery method that can achive high concentration of IL-12 specifically in cancerous microenvironments. In mice tumour-models, this novel molecule achieved a CR rate of up to 67% for melanoma, and 87% for breast cancer when combined with CPI drugs (a mix of both anti-PD1 and anti-CTLA4). While these results are very encouraging, the study showed that such high CR-rates could only be achieved in very specific settings (such as a tumour volume of 70mm^3 upon injection). Different settings (e.g. volume of 150mm^3) elicited little to no response. This heterogeneity of treatment outcome could not be explained. The first step to improve efficacy of CBD-IL-12-based treaments would thus be to understand better what are the key parameters that control the treatment outcome.

1.3 Experimental Data

Add some plots here.

1.4 Previous Work on Computational Modelling

[§ about why mechanistic models are useful]

To this end, T. Miyano (2019), under the supervision of R. Tanaka, proposed to use a computational modelling approach to the problem. He developped an initial mechanistic model based on Delay-Differential Equations (DDEs), parameterised by 21 parameters representing various relevant biological factors of a given mouse, such as the tumour growth rate or the degradation rate of IFNγ [17]:

$$
\begin{aligned}
\dot{g}(t) &= k_1 + k_2[d_{CBD}(t) + d_{12}(t)] - d_1 g(t) \\
\dot{c}(t, t-t_d) &= k_3 + k_4 g(t-t_d) - d_2 c(t) \\
\dot{p}(t) &= k_5 - [d_3 + d_4 g(t)]p(t) \\
\dot{v_l}(t) &= k_6 \left[1 - \frac{v(t)}{v_{max}}\right] v_l(t) - \left[d_5 + \frac{\frac{d_6 c(t)}{1+s_1 p(t)(1-d_{CPI}(t))} + d_7 g(t)}{1 + s_2 v(t)}\right] v_l(t) \\
\dot{v_d}(t) &= \left[d_5 + \frac{\frac{d_6 c(t)}{1+s_1 p(t)(1-d_{CPI}(t))} + d_7 g(t)}{1 + s_2 v(t)}\right] v_l(t) - d_8 v_d(t)
\end{aligned}
$$

The five state variables (g, c, p, v_l and v_d) are concentration of IFNg, of CD8+ and of PD1 along with volume of living and dead tumour, respectively. This was motivated by the fact that these are the key players in the immune response, as explained above. The meaning of each parameter is reported in the Appendix. The model was investigated by C. Hines, who showed that the model could successfuly

reproduce experimental data by using a Genetic Algorithm for parameter fitting [18]. However, C. Hines also demonstrated in a subsequent analysis that the model was conflicting with findings from the biologists in two ways. A positive feedback loop, where IL-12-induced IFNg in turn produces IL-12, is missing from the model [19]. Additionally, C. Hines showed that the model outcome does not depend much on the initial tumour volume and treatment characteristics (day of injection, number of doses, etc.)[18], which is opposite to results reported in [15]. Rather, he found that the model depends almost exclusively on parameter k_6, d_1 and s_2 (which respectively corresponds to proliferation rate of tumour; degradation rate of IFNg and tumour-induced immunosuppression strength)

1.5 Aims and Objectives

The aim of the cancer immunotherapy project is to use computational models to improve our understanding of the immune mechanisms behind the CBD-IL-12 immunotherapy, utlimately to characterise the responder profile for the treatment.

Objective 1: change the initial mechanistic model to a Bayesian model so that it can reproduce the experimental data while including all the important pathways of the immune response.
Objective 2: identify key biological factors in mice that determine the outcome of the treatment, along with the corresponding threshold that separates complete response (CR) from non-CR
Objective 3: associate key factors to potential biomarkers in mice
Objective 4: *(potential!)* understand how the boundary between CR and non-CR depends on the treatment characteristics (number and frequency of doses, combination with other treaments, etc.)

2 Ethical Analysis

Lorem ipsum dolor sit amet, consectetuer adipiscing elit. Ut purus elit, vestibulum ut, placerat ac, adipiscing vitae, felis. Curabitur dictum gravida mauris. Nam arcu libero, nonummy eget, consectetuer id, vulputate a, magna. Donec vehicula augue eu neque. Pellentesque habitant morbi tristique senectus et netus et malesuada fames ac turpis egestas. Mauris ut leo. Cras viverra metus rhoncus sem. Nulla et lectus vestibulum urna fringilla ultrices. Phasellus eu tellus sit amet tortor gravida placerat. Integer sapien est, iaculis in, pretium quis, viverra ac, nunc. Praesent eget sem vel leo ultrices bibendum. Aenean faucibus. Morbi dolor nulla, malesuada eu, pulvinar at, mollis ac, nulla. Curabitur auctor semper nulla. Donec varius orci eget risus. Duis nibh mi, congue eu, accumsan eleifend, sagittis quis, diam. Duis eget orci sit amet orci dignissim rutrum.

3 Litterature Review

To identify the patterns within the set of biological factors that can differentiate CR from non-CR, we must first estimate the value of these factors from the data, since they cannot be directly measured experimentally. This hence gives rise to a first problem, which is to perfom parameter estimation on a DDE model. In the context of non-linear pharmacodynamics model, an article by Sonnet et al, 2013 [20], provides a review of the different techniques available along the set of assumptions they rely on. For analysis of population data with observational noise, three methods can be explored: Stochastic Expectation-Maximisation (EM), First-Order Conditional Estimation (FOCE) and Bayesian modelling. While they were shown to have similar performances were some specific problem [cite], in our case we expect a Bayesian approach to perform better since ...

3.1 Bayesian Parameter Estimation

Let the general definition of a Delay-Differential Equations (DDE) model be:

$$\frac{\mathrm{d}X_i}{\mathrm{d}t} = f_i(t, \boldsymbol{X}(t), \boldsymbol{X}(t-\tau)|\boldsymbol{\theta}), \qquad t \in [t_0, t_{max}], i = 1, \ldots, I$$

where τ denotes a constant delay, so that the rate of change of state X_i depends on both the present state $\boldsymbol{X}(t)$ and a past state $\boldsymbol{X}(t-\tau)$. The subscript i indexes the different state variables of interest, and $\boldsymbol{\theta}$ is the (unknown) vector of the parameters for the DDE model. We must bear in mind that this parameter vector is different for each treated mouse, as it uniquely characterises its treatement response, and hence we denote with $\boldsymbol{\theta}_j$ the parameter vector that characterises the j-th mouse. The experimentally observed tumour evolution for the j-th mouse is denoted by $\boldsymbol{y}_j$, and each element is the tumour volume observed at a given time.

Bayesian Parameter Estimation is a method to estimate $\boldsymbol{\theta}_j$ given an observation vector $\boldsymbol{y}_j$. Contrary to frequentist approach, estimations are in the form of probability distributions (called posteriors, denoted $p(\boldsymbol{\theta}|\boldsymbol{y})$) rather than point estimates.

For a situation where data about only one individual was gathered, the posterior distribution is defined as follows [cite txtbook]:

$$p(\boldsymbol{\theta}|\boldsymbol{y}) \propto p(\boldsymbol{\theta})p(\boldsymbol{y}|\boldsymbol{\theta})$$

This formula is the direct application of Bayes' theorem. It is the product of the prior distribution $p(\boldsymbol{\theta})$, which represents our knownledge of the problem, and the likelihood $p(\boldsymbol{y}|\boldsymbol{\theta})$. Before further defining these distributions, we must extend this definition of the posterior distribution to work for mixed-effects models.

3.2 Hierarchical Modelling

We seek to estimate the probability distribution of the parameter vector $\boldsymbol{\theta}$ for each treated mouse, however these vectors are not independent from each other since they come from the same mouse species. The use of a hierarchical model enables us the formulate that the parameter vector is sampled from an population-level distribution characterised by the (also unknown) hyperparameters $\boldsymbol{\phi}$. The objective is hence to find

the distribution of both $\boldsymbol{\theta}_j$ $\forall j$ and $\boldsymbol{\phi}$. The Bayesian parameter estimation framework integrates this additional assumption by changing the posterior to [cite txtbook again]:

$$p(\boldsymbol{\theta}, \boldsymbol{\phi}|\boldsymbol{y}) \propto p(\boldsymbol{\phi})p(\boldsymbol{\theta}|\boldsymbol{\phi})p(\boldsymbol{y}|\boldsymbol{\theta})$$

This expression is a product of the hyperprior $p(\boldsymbol{\phi})$, the population distribution $p(\boldsymbol{\theta}|\boldsymbol{\phi})$ and the likelihood $p(\boldsymbol{y}|\boldsymbol{\theta})$. In the following part, we explain in more details how these distributions are defined.

3.2.1 Likelihood function

Assuming that the observational noise is a white Gaussian noise with zero-mean and a standard deviation σ_{err} that is common to all experiments, the likelihood can then be defined as follows [21], [22] (for a given tumour evolution $\boldsymbol{y}_j$):

$$\mathcal{L}(\boldsymbol{\theta}_j) = \prod_{t=t_0}^{t_{max}} \frac{1}{\sigma_{err}} \exp\left(-\frac{(y_j(t) - Y_j(t|\boldsymbol{\theta_j}))^2}{2\sigma_{err}^2}\right)$$

3.3 Reduction of the Computational Burden

3.3.1 Sensitivity Analysis

As pharmacodynamics model can be high dimensional, the Bayesian approach, which is computationally intensive [20], can result in intractable computations. To this end, Vasquez-Cruz et al, 2012 [23], proposed a method to reduce dimensionality of system biology models. By taking the example of a crop growth ODE model with 17 parameters, they used a senstivity analysis (namely, eFAST and Sobol' method) to identify the most influencial parameters, and used these results to design a reduced model with only 7 free parameters. Then, using a parameter fitting algorithm, they were able to show that this reduced model could still replicate the experimental data with minimal error. Additionally, they showed that the two sensitivity analysis methods (eFAST and Sobol' methods) yield different results and hence need to be combined together.

3.3.2 High-performance Computational Methods

As the estimation of the posterior distributions cannot be evaluated analytically, Luengo et al., 2020 [24], pointed out that Markov-Chains Monte Carlo approach to approximate the posterior is the only feasible approach in most applications. While many different MCMC methods exist [25], it was shown by Nishio et al, 2019 [26] that the No U-Turn Sampler (NUTS) led to lower skewness of the posterior and more decorrelated samples compared to the other two popular algorithms, Gibbs and Hamiltonian Monte Carlo samplers. However, traditional MCMC methods, including NUTS, performs badly to estimate multimodal posterior distributions [**?**]. Liu et al, 20

4 Implementation Plan

5 Risk Register

The main risks are :

Risk	Likelihood	Impact	Mitigation Strategy
not finishing the project	?	?	?

Table 1: Table of the different risks associated with the project's objectives

6 Evaluation

Below we present a list of the key components of the cancer immunotherapy project, along with a way to verify that they function correctly. The Bayesian encompasses the mechanistic model, as the likelihood function.

Mechanistic Model

The mechanistic model is the core element of the project. Its 'quality" can be asessed by two criteria: it should be able to reproduce the data obtained in the lab by Dr. Ishihara (see Appendix), and it should make "biological sense". To assess the former, we propose to use the standard method of parameter fitting through a Genetic Algorithm (GA), which has already been used in the past for this purpose [19]. This enables us to find a parameterisation of the model that leads to the best simulation, along with the Mean-Squared Error to the true data. This metric can be used to validate that the model can produce data close enough to the experimental time series. To assess the second criteria, we will use a sensitivity analysis (namely, the eFAST method [should justify?]). It enables us to check that the model is sensitive to the same quantity as shown in the lab [wording is terrible here, need to rephrase], for example to the treatment specification or to the initial tumour volume, which is not the case for the current one. [need to describe experiments more?]

Bayesian Model

To validate the Bayesian model, which is an extension of the mechanistic model, we will follow the Bayesian Workflow procedure, as explained on Section 4. Each validation test is evaluated differently:

- **Prior Predictive Check:** we sample 1,000 sets of parameter from the priors and simulate tumour growth for each of them. The 95% credible interval of the resulting collection of time series should contain our expected range of curves we can expect. Evaluation of this step is mostly qualitative.
- **Fake Data Check:** we first need to generate a artificial dataset using known values of parameters, and then fit the Bayesian model to these fake datasets. By comparing the results of the model (i.e. the estimated parameter value in the form of the posterior distribution) to the true values, we can conclude whether the model can successfully perform parameter estimation or not. A possible quantitative approach detailed in [27] involves substracting the true parameter value from the posterior. This results in a "error" distribution that should theoretically be zero-mean.
- **Posterior Predictive Check:** this is analogous to the Prior Predictive Check, except that parameter are drawn from the posterior distributions instead of the prior distributions. This results in a collection of simulated time series. The median curve can be compared with the true curve obtained in the lab through a difference metric (MSE is the typical error metric for time series).

Responder Profile

Once the responder profile has been characterised, its accuracy can be evaluated by comparing the predicted treatment outcome against the true outcome on a new batch of cancerous mice. The procedure to inoculate skin cancer, inject the immunotherapy and measure tumour volume should be the same as defined in [15] and [17]. To be robust against all cases, only half of the batch of cancerous mice should be predicted as complete responder according to the responder profile. This ensures that we can collect data about the accuracy for both true positives and of true negatives.

7 Preliminary Results

7.1 Numerical Stability Analysis

[Figures are missing but they will be added soon]
The very first aspect of Miyano's model that we wanted to verify was its ability to capture two specific treatment outcome: CR vs non-CR. As these behaviours can essentially be characterised by the fixed-points of the model (if the steady-state behaviour of the model converges to high values of tumour volume, it is a non-CR behaviour, and vice-versa). We opted for a grid-search stability analysis, meaning that we sample reguarly-spaced points in parameter space and classify them as either CR or non-CR. Fig. X shows the resuls of this analysis, where each axis of corresponds to the value of a lnk6, lns2 or lnd1 respectively. A can be seen, there seem the be a clear boundary between the two response modes, with very little "mixing". This suggests that it would be possible to predict how a given patient would respond to the treatment, by knowning on which side of the boundary he is.

7.2 Sensitivity Analysis

In order to restrict the parameter space for subsequent analysis, and also to understand to main mechanisms behind the immune response, we performed a eFAST sensitivity analysis, which is a variance decomposition method. As it can only decompose variance of a scalar metric, it does not nateivly support time-series. Hence we chose to apply it to the integral of the tumour growth curve simulated by Miyano's model. Results are shown in Fig. 1. The total height of the bar represent the fraction of the variance that is imputable to the corresponding parameter. The first observation we can make is that model is mostly sensitive to k_6, d_1, d_7 and s_2. However, seen, we can see that the main effect indices (in blue) are almost always negligible compared to the interaction indices (orange). According to a study by Vazquez-Cruz et al. (2012), this is a typical sign of non-identifiability [23] that will significantly hinder Bayesian inference. Additionally, results indicate that the treatment characteristics (labelled `tem`, `td` and `ti`) have almost no impact on the treatment outcome, which is conflicting with the results experimentally obtained in the CBD-IL-12 study [15].

7.3 Bayesian Model Validation

In this section we show how the Bayesian model was validated, following the procedure highlighted in Sections **??** and 4. We focus on a reduced model with only three free parameters, k_6, d_1, s_2, which were identified by C. Hines are the most impactful ones [18]. All other parameters of the model were fixed to arbitrary, "realistic" values.

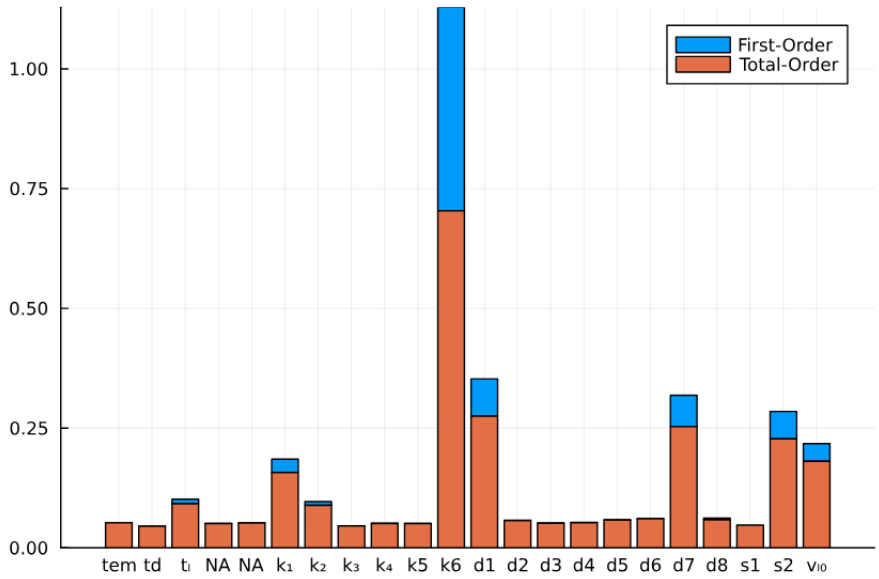

Figure 1: Results of the eFAST sensitivity analysis on the initial model

7.3.1 Prior Predictive Check

In this case, we do not have much data on the typical values of the parameters since it is impossible to measure it (we only know that it is a positive number whose typical value is between 0 and 1, as evidenced by [18]), so we aim to design an uninformative prior. Fig. 2 shows a plot of 1,000 tumour growth time-series. Each of them was simulated using a set of parameters drawn from the following prior distribution:

$$\ln(k_6) \sim \text{Cauchy}^-(0, 1)$$
$$\ln(d_1) \sim \text{Cauchy}^+(0, 1)$$
$$\ln(s_2) \sim \text{Cauchy}^-(0, 1)$$

As we exponentiate the Cauchy distribution, it means that $0 < k_6 < 1$. The blue shade represents the 95% credible interval, and the dark green line is the median growth curve. As we can see, the 95% credible interval is very wide and can virtually contain our expected range of curves, since it ranges from 0 (minimum volume) to 600 (maximum possible volume according to the equation), meaning that they are relatively uninformative priors. The median curve has the shape of the typical growth curve, as observed in the labs. Hence, we can say that the prior distribution is satisfying, as it could explain any potential growth curve while restricting the values of the parameters to a smaller subset of $\mathbb{R}$.

7.3.2 Fake Data Check

Each fake growth curve was generated by sampling a value of θ from the prior distribution, and then simulating the tumour growth in the same way as for the Prior Predictive Check. However, as biological data is always noisy, we also added some noise to make the fake dataset closer to what we would actually expect from the labs. This was done in two different ways, resulting in two distinct datasets. For dataset

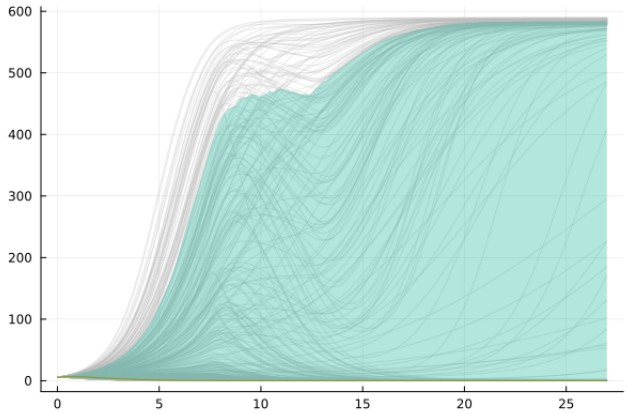

Figure 2: ODE solution for 1,000 parameter values sampled from the prior ($\boldsymbol{\theta} \in \mathbb{R}^1$)

A, we simply added a white standard Gaussian noise to the simulation. For dataset B, we use added white noise to the log of the simulated curve. The generation process is summarized in Table 2, where x_* denotes a noiseless data point. The reason for using two different noise generation is that we observed, in the experimental data from the labs, that data points are usually more dispersed when they have a high value, suggesting an exponential relationship.
Additionally, each dataset contains 10 time series. Fig. 3 plots the fake data points against the original curve. For clarity, only 5 time series, selected at random, were shown. *Results*

Table 2: Summary of the generation process for the two datasets A and B

Dataset	Generation Process
A	$x_A = x_* + \mathcal{N}(0, 1)$
B	$x_B = x_* \times e^{\mathcal{N}(0, 0.3)}$

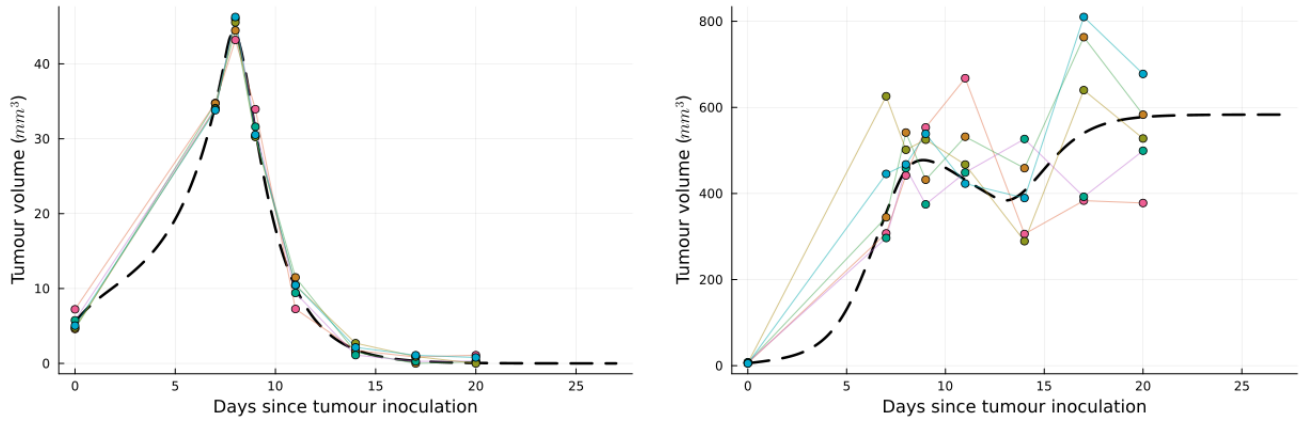

(a) Dataset A

(b) Dataset B

Figure 3: Plot of the fake data points (colored lines and scatter plot) along with the original growth curve (dashed line)

Before checking if the estimated values match the true ones, we first assess convergence of the MCMC chains. Th R-hat values are reported in Table. 3 as the average R-hat value accross the 3 parameters. It must be noted that in this case, for a given inference, some chains get trapped while some are well-mixed. In that case, the R-hat calculation excludes the trapped chains. This is indicated in the Tables by reporting the number of chains used to calculate R-hat (out of the 5 chains). If none of the chain converged, we simply report N/A. Looking at Table 3, we can hence conclude that the chains did not

Table 3: Assessement of convergence for the MCMC chains for uninformative priors (3 free parameters)

Data set	Pooling Type	R-hat diagnostic	Number of Chains	Convergence
A	None	116.08	N/A	No
	Complete	298.67	N/A	No
B	None	1.092	3/5	Close to
	Complete	3.11	N/A	No

converged, meaning that the model cannot make inference with $\boldsymbol{\theta} \in \mathbb{R}^3$ and uninformative priors. To further diagnose the model, we performed another set of inferences, except that the priors where highly informative:

$$\begin{aligned}\ln(k_6) &\sim \text{Cauchy}^-(\theta_{k_6}, 1)\\ \ln(d_1) &\sim \text{Cauchy}^+(\theta_{d_1}, 1)\\ \ln(s_2) &\sim \text{Cauchy}^-(\theta_{s_2}, 1)\end{aligned}$$

where θ_x represent the true value of parameter x. Convergence of this new set of inferences is shown in Table 4. As we can see, convergence of the MCMC chains are still very poor, even with highly informative priors centered on the true parameter values.

Table 4: Assessement of convergence for the MCMC chains for uninformative priors (3 free parameters)

Data set	Pooling Type	R-hat diagnostic	Number of Chains	Convergence
A	None	18.15	N/A	No
	Complete	45.96	N/A	No
B	None	1.505	3/5	Close to
	Complete	1.014	2/5	Yes

It might be objected that Cauchy distributions are by definition not too informative since a non-negligible portion of their mass stretches well beyond their standard deviation, contrary to normal distributions. This hence motivated us to perform one last fake data check, using the normal priors shown below to be even more informative:

$$\begin{aligned}\ln(k_6) &\sim \mathcal{N}^-(\theta_{k_6}, 0.3)\\ \ln(d_1) &\sim \mathcal{N}^+(\theta_{d_1}, 0.3)\\ \ln(s_2) &\sim \mathcal{N}^-(\theta_{s_2}, 0.3)\end{aligned}$$

Convergence results are shown in Table. 5. The main result is that chains converged or were close to convergence only for dataset D, showing that a log-normal transformation is key to make exploration of the posterior easier to perform. Whilst the overall convergence rate is still very low given the informative normal priors, this series of fake data checks for the case of three free parameters highlighted the key role of the log-transformation.

Table 5: Assessement of convergence for the MCMC chains for uninformative priors (3 free parameters)

Data set	Pooling Type	R-hat diagnostic	Number of Chains	Convergence
A	None	7.387	N/A	No
	Complete	39.17	N/A	No
B	None	1.066	3/5	Yes
	Complete	1.111	5/5	Close to

Conclusion

Even with informative priors, the MCMC chains do not even converge. This suggests that the likelihood function is too difficult to explore and might contain discontinuities. As suggested by Gelman et al. (2020) in their *Bayesian Workflow* document, the first step to take to address this issue would be to drastically simplify the likelihood function and re-assess performance of the model of fake datasets. Another approach that we are currently exploring would be to use Approximate Bayesian Computation.

References

[1] Jiaquan Xu et al. Mortality in the United States. *NCHS Data Brief*, 2021.

[2] Kim S.Ka. and Cho S.W. The evasion mechanisms of cancer immunity and drug intervention in the tumor microenvironment. *Front Pharmacol.*, 13(868695), 2022.

[3] I.L. Jr Bennet and P.B. Beeson. Studies on the pathogenesis of fever - characterization of fever-producing substances from polymorphonuclear leukocytes and from the fluid of sterile exudates. *J Exp Med.*, 98:493–508, 1953.

[4] R. Mortarini, A. Borri, G. Targni, et al. Peripheral burst of tumor-specific cytotoxic T lymphocytes and infiltration of metastatic lesions by memory CD8+ T cells in melanoma patients receiving interleukin 12. *Cancer Res.*, 60:3559–68, 2000.

[5] J.E. Portielje, C.H. Lamers, W.H. Kruit, A. Sparreboom, R.L. Bolhuis, G. Stoter, et al. Repeated administrations of interleukin (IL)-12 are associated with persistently elevated plasma levels of IL-10 and declining IFN-gamma, tumor necrosis factor-alpha, IL-6, and IL-8 responses. *Clin Cancer Res*, 9, 76-83.

[6] A. Mukhopadhyay, J. Wright, S. Shirley, D.A. Canton, C. Burkart, R.J. Connolly, et al. Characterization of abscopal effects of intratumoral electroporation-mediated IL-12 gene therapy. *Gene Ther.*, 26:1–15, 2019.

[7] B.V. Kumar, T.J. Connors, and D.L. Farber. Human T cell development, localization, and function throughout life. *Immunity*, 48:202–213, 2018.

[8] L.K. Chen, B. Tourvieille, G.F. Burns, F.H. Bach, D. Mathieu-Mahul, M. Sasportes, and other. Interferon: a cytotoxic T lymphocyte differentiation signal. *Eur J Immunol*, 17, 767-70.

[9] Y. Hayakawa, K. Takeda, H. Yagita, M.J. Smyth, L. Van Kaern, K. Okumura, et al. IFN-gamma-mediated inhibition of tumor angiogenesis by natural killer T-cell ligand, alpha-galactosylceramide. *Blood*, 100, 2002.

[10] F.M. Rosa, M.M. Cochet, and M. Fellous. Interferon and major histocompatibility complex genes: a model to analyse eukaryotic gene regulation? *Interferon*, 7:47–87, 1986.

[11] S.A. Rosenberg, B.S. Packard, P.M. Aebersold, D. Solomon, S.L. Topalian, S.T. Toy, et al. Use of tumor-infiltrating lymphocytes and interleukin-2 in the immunotherapy of patients with metastatic melanoma. *N Engl J Med*, 319:1676–80, 1988.

[12] B.T. Fife and J. A Bluestone. Control of peripheral T-cell tolerance and autoimmunity via the CTLA-4 and PD-1 pathways. *Immunol. Rev*, 224:166–182, 2008.

[13] B.T. Fife and J.A. Bluesone. Control of peripheral T-cell tolerance and autoimmunity via the CTLA-4 and PD-1 pathways. *Immunol. Rev.*, 224, 166-182.

[14] H. Nishimura, N. Minato, T. Nakano, and T. Honjo. Immunological studies on PD-1 deficient mice: implication of PD-1 as a negative regulator for B cell responses. *Int Immunol*, 10:1563–72, 1998.

[15] A. Mansurov, J. Ishihara, P. Hosseinchi, et al. Collagen-binding il-12 enhances tumour inflammation and drives the complete remission of established immunologically cold mouse tumours. *Nature Biomedical Engineering*, 4:531–543, 2020.

[16] Shuaishuai Xu, Huaxiang Xu, Wenquan Wang, et al. The role of collagen in cancer: from bench to bedside. *J Trans Med*, 17(309), 2019.

[17] Takuya Miyano. Mathematical modeling of complete remission of immunologically cold tumor by tumor-matrix targeted interleukin-12, 2019.

[18] Christian Hines. Cancer immunotherapy meeting notes, 2022.

[19] Christian Hines. Positive feedback between IL-12 and IFNg, 2022.

[20] Sophie Donnet and Adeline Samson. A review on estimation of stochastic differential equations for pharmacokinetic/pharmacodynamic models. *Advanced Drug Delivery Review*, 65, 2013.

[21] Baisen Liu, Liangliang Wang, and Jiguo Cao. Bayesian estimation of ordinary differential equation models when the likelihood has multiple local modes. *Monte Carlo Methods and Applications*, 24(2):117–127, 2018.

[22] Valderrama-Bahamóndez, Gloria I., and Holger Fröhlich. Mcmc techniques for parameter estimation of ode based models in systems biology. *Frontiers in Applied Mathematics and Statistics*, 5, 2019.

[23] M.A. Vazquez-Cruz, R. Guzman-Cruz, I.L. Lopez-Cruz, et al. Global sensitivity analysis by means of efast and sobol' methods and calibration of reduced state-variable tomgro model using genetic algorithms. *Computers and Electronics in Agriculture*, 100, 2014.

[24] D. Luengo, L. Martino, M. Bugallo, et al. A survey of monte carlo methods for parameter estimation. *EURASIP J. Adv. Signal Process*, 25, 2020.

[25] C.P. Robert and W. Changye. Markov chain monte carlo methods, a survey with some frequent misunderstandings, 2020.

[26] Motohide Nishio and Aisaku Arakawa. Performance of hamiltonian monte carlo and no-u-turn sampler for estimating genetic parameters and breeding values. *Genetics Selection Evolution*, 51(73), 2019.

[27] B. Rosenbaum, M. Raats, et al. Estimating parameters from multipple time series of population dynamics using bayesian inference. *Frontiers in Ecology and Evolution*, 6(234), 2019.